Current concepts and future perspectives on surgical optical imaging in cancer

Vasilis Ntziachristos
Jung Sun Yoo
Technische Universität München
Helmholtz Zentrum München
Institute for Biological and Medical Imaging
Munich, Germany 80333

Gooitzen M. van Dam
University of Groningen
University Medical Center Groningen
Division of Abdominal and Surgical Oncology
Department of Surgery
BioOptical Imaging Center Groningen
Groningen, The Netherlands 9700 RB

Abstract. There are vibrant developments of optical imaging systems and contrast-enhancing methods that are geared to enhancing surgical vision and the outcome of surgical procedures. Such optical technologies designed for intraoperative use can offer high integration in the operating room compared to conventional radiological modalities adapted to intraoperative applications. Simple fluorescence epi-illumination imaging, in particular, appears attractive but may lead to inaccurate observations due to the complex nature of photon-tissue interaction. Of importance therefore are emerging methods that account for the background optical property variation in tissues and can offer accurate, quantitative imaging that eliminates the appearance of false negatives or positives. In parallel, other nonfluorescent optical imaging methods are summarized and overall progress in surgical optical imaging applications is outlined. Key future directions that have the potential to shift the paradigm of surgical health care are also discussed. [DOI: 10.1117/1.3523364]

Keywords: cancer; intraoperative imaging; near-infrared fluorescence; optical imaging; tumor; resection margin; lymph node detection.

Paper 10279VR received May 25, 2010; revised manuscript received Sep. 24, 2010; accepted for publication Oct. 11, 2010; published online Dec. 29, 2010.

1 Introduction

Optical imaging is the primary surgical visualization modality by means of the surgeon's visual perception. Similarly, optical microscopes have been adapted to surgical systems for improving resolution. Human vision is however significantly limited to visualizing only superficial contrast. In addition, despite its ability to efficiently recognize anatomical features, human vision can distinguish only a relatively small number of spectral features and virtually no molecular-based features, which results in reduced contrast for separating cancer from surrounding tissue. The emergence of fluorescence imaging offers a potent modality for improving the surgical outcome, by imparting specific functional and molecular contrast and by allowing penetration of several millimeters to centimeters into tissue. In addition, elaborate spectral imaging or high-resolution methods have shown potential for accurately distinguishing tissue fluorochromes and improving the physiological information available to the surgeon.

Many of the original systems described for intraoperative optical imaging operated as modifications to surgical microscopes or as epi-illumination (photography/video) fluorescence systems. In addition, the use of nonspecific dyes enhanced visualization of vasculature and abnormal vessel permeability but failed to accurately correlate with remnant disease or locoregional microfoci. More recently, there is shift toward engineering novel contrast mechanisms, typically based on targeting molecular features of cancer cells. In addition, advanced optical technology based on image correction for tissue attenuation variation, hyperspectral methods, optical coherence tomography, or optoacoustics are considered for improving surgical visualization over human vision or photography. This *review* illuminates developments in intraoperative optical imaging strategies and technical advancements. Particular weight is given to discussing novel trends that can account for the various effects of photon-tissue interactions and reduce the number of false positives and false negatives that may be present in simple epi-illumination (photographic) imaging approaches. Imaging examples and applications are summarized, and highly promising directions for clinical propagation are outlined (see Table 1).

2 Intraoperative Imaging Using Organic Fluorescent Dyes

Since the original use of fluorescein in the 1940s and 1950s,[1,2] several fluorochromes, including fluorescent photosensitizers, have been investigated for their ability to enhance margin delineation, including indocyanine green (ICG),[3] fluorescein-albumin,[4] and porphyrins.[5,6] ICG and fluorescein dyes[7] are nonspecific dyes with a long history of clinical use. Both dyes are general markers of blood pooling because they are bound to serum proteins and outline the vascular system. As such, they are used to outline areas of perfusion and areas of high vascular permeability (leakage), such as in eye angiography, although some photochemical limitations have been noted.[8] Other uses and indications have been described, spanning from microscopy uses in cellular biology to hepatic and cardiac function studies. ICG absorbs light with a maximum at 805 nm and exhibits

Address all correspondence to: Vasilis Ntziachristos, Technische Universität München, Helmholtz Zentrum München, Institute for Biological and Medical Imaging, Munich, Germany 80333; Tel: 49-89-3187 4139; Fax: 49-89-3187 3017; E-mail: v.ntziachristos@tum.de

1083-3668/2010/15(6)/066024/12/$25.00 © 2010 SPIE

Table 1 Optical imaging systems considered for surgical imaging.

Technology	Resolution	Quantification	Maximum depth of operation	Example Refs.
Modified microscope	5–10 μm[a]	N/A	0.1 mm	9, 19
OCT	1–10 μm	N/A	1 mm	62, 65
Epi-illumination imaging/video	20μ–5 mm[b]	No	>1 cm	11, 13
Epi-illumination imaging/video with color	20μ–5 mm[b]	No	>1 cm	14, 15
SFI with correction	20μ–5 mm[b]	Yes	>1 cm	23, 24
Optoacoustic imaging	50–200μ	Yes	>1 cm	76, 78

[a]This resolution is reported for imaging tissue *in vivo* using conventional microscopy. Confocal or two-photon methods can reject out-of-focus contributions and offer diffraction-limited resolution.
[b]Resolution in epi-illumination imaging approaches depends strongly on the depth of operation. 20μ is reported for superficial imaging in the visible, but the resolution drops significantly when imaging signals from deeper in tissues.

maximum fluorescence emission at 835 nm, whereas fluorescein absorbs light with a maximum at 494 nm and fluoresces with a maximum at 591 nm. Therefore, ICG is suited for deep-tissue imaging, because the near-infrared wavelengths (i.e., 650–950 nm) are attenuated significantly less than the visible wavelengths by tissue, and penetration depths on the order of several centimeters can be achieved. Other nonspecific dyes have also been explored in different intraoperative applications, as described in the following. Typically, modified microscopes have been used for visualization as shown in Fig. 1. Modifications span from the use of appropriate light sources and filters to appropriately excite different fluorochromes of interest to advanced spectral imaging and custom made additions that significantly improve imaging performance as outlined in the following.

2.1 *Tumor Delineation*

Intraoperative imaging studies involving ICG or fluorescein have been performed for outlining gliomas. Kuroiwa et al.[9] reported on a fluorescence imaging system that modified a Zeiss OPMI surgical microscope using appropriate filters for illumination and selection of signals emitted from fluorescein, employed for glioma surgery. Fluorescein was employed to outline areas of blood-brain barrier disruption due to invasive tumors. Significant fluorescence enhancement was seen from tumors compared to surrounding tissues; however, no analytical results on remnant disease or follow-up studies were carried out in the study. Figure 2 shows pre- and postoperative MRI images, intraoperative anatomy and fluorescence images, and correlative histology from the brain surface of human who suffered malignant glioma resection by aid of this setup. In a similar implementation, Haglund et al. employed ICG for determination and resection of glioma margins in rat[10] and human[3] brain. The imaging system used a 100-W tungsten-halogen bulb as an excitation light source, filtered using a long-pass interference filter to select light of >690-nm wavelengths. Imaging was performed to outline primary tumor margins and remnant disease after tumor resection. The study observed similar contrast enhancement from the tumor area and different ICG-clearance kinetics between the malignant and nonmalignant areas. Optically guided microscopic resection demonstrated 93% specificity and 89.5% sensitivity in tumor detection.

2.2 *Organ Viability*

Besides the delineation of tumor borders, ICG has been further used in the intraoperative evaluation of organ viability. Holm

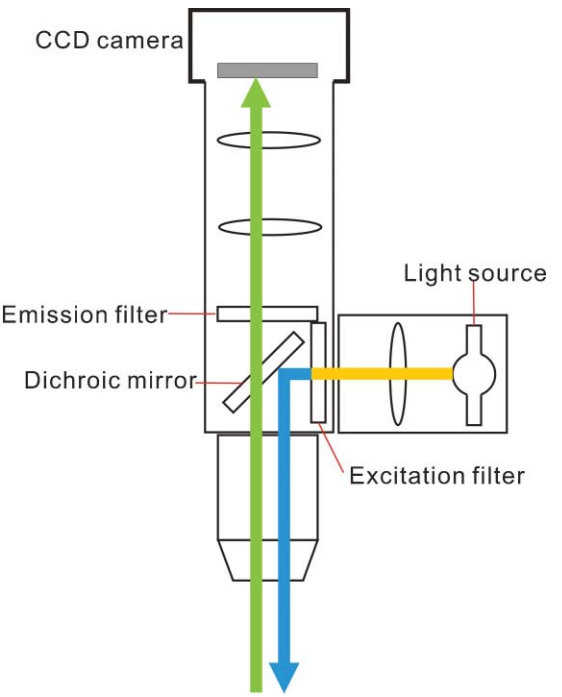

Fig. 1 Schematic representation illustrating modified epi-illumination microscope system for intraoperative fluorescence imaging. Light from a light source is filtered at wavelengths appropriate for excitation of the fluorochrome of interest and directed to the specimen through the microscope objective using a dichroic mirror. Fluorescence light emitted from tissue is collected from the same objective, filtered by the emission filter, and detected using a CCD camera.

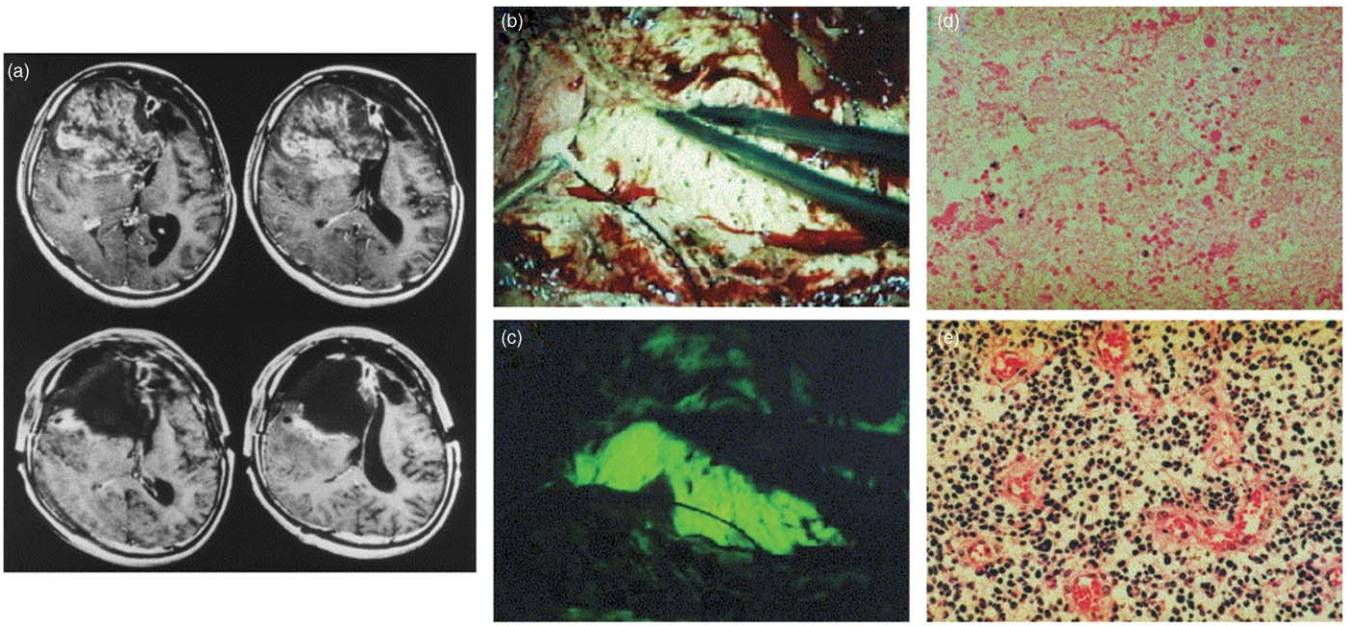

Fig. 2 Human malignant glioma surgery using fluorescein imaging: (a) Preoperative (upper) MRI image showing a large tumor enhancing in the right frontal lobe and postoperative (lower) MRI image with no enhanced tumor; (b) intraoperative image of anatomical vision using ordinary microscope; (c) intraoperative image of fluorescein from brain tumor using modified microscope for fluorescence imaging; (d) histological examination of nonfluorescence area, which is found as a necrotic area; and (e) histological examination of fluorescence area, which shows a significant number of tumor cells.

et al.[11] for example, have employed ICG to determine the efficacy of skin-flap perfusion, while Kubota et al.[12] assessed the success of blood-vessel reconstruction in living-donor liver transplantation patients. Similarly, Takahashi et al.[13] employed ICG imaging for the evaluation of graft patency of patients during off-pump coronary artery bypass grafting. Imaging in these applications was based on commercially available epi-illumination near-infrared (NIR) imaging systems operating in video mode, using appropriate excitation light for ICG and cutoff filters for fluorescence detection.

Nakayama et al.[14] have also developed a video system for intraoperative imaging of small animals and demonstrated intraoperative visual assessment of cardiac muscle viability in rats using the IRDye78-CA and the IR-786 NIR dyes. The IRDye78-CA stays intravascular and exhibits rapid distribution and clearance to delineate blood flow *in vivo*, whereas the IR-786 was employed to assess myocardial perfusion. The system developed combined color and NIR fluorescence views that run in parallel to achieve real-time imaging. NIR excitation was via a custom 771-nm, 250-mW laser diode system at a fluence rate of 50 mW/cm^2. White-light excitation was also employed via a 150-mW halogen lamp, depleted of wavelengths greater than 700 nm. Data were acquired assuming sequential injection of dyes because a single excitation wavelength was employed. Occluded vessels and a blood defect were visible in the NIR. Potential application of the technology was assumed to be the possible guiding of revascularization or the assessment of the biodistribution of targeted gene therapy to specific myocardial regions. A similar system, developed by De Grand and Frangioni[15] utilized halogen sources instead of laser diodes to generate 5 mW/cm^2 NIR excitation light over a 20-cm-diam surgical field and was similarly employed to visualize vascular perfusion in 35-kg pigs using ICG. Figure 3 shows the setup and an intravascular mapping image of the coronary circulation.

2.3 *Lymphatic Imaging*

Lymph-node mapping has also been considered in intraoperative imaging using NIR organic dyes.[16–18] Parungo *et al.*[16,17] and Tanaka et al.[18] used a system similar to the one shown in Fig. 3(a) to image the NIR fluorophores HSA-78 and HSA800. HSA-78 was made of human serum albumin (HSA) covalently conjugated to the IRDye78 (LI-COR, Lincolin, NE), whereas HSA800 was also made of HSA covalently conjugated to the CW800 fluorochrome (LI-COR, Lincolin, NE). Both molecules exhibited similar characteristics, with HSA800 attaining a hydrodynamic diameter of 7.4 nm, and 784- and 802-nm excitation and emission wavelengths, respectively, and HSA-78 having 7 nm of hydrodynamic diameter and 778 nm, 795 nm excitation and emission peak respectively. HSA-78 and HAS800 were found in two or more draining nodes compared to larger moieties, such as quantum dots, which migrated only to the first draining lymph node. Tanaka et al.[18] also considered a modified dual-camera video system with fluence rates for NIR and white-light imaging in the range of 0–5 and 0–1 mW/cm^2, respectively. Spatial resolution at the field of view (FoV) of 20 $\times$ 15 cm was 625 μm and, at a FoV of 4 $\times$ 3 cm, was 125 μm. Using this system, sentinel lymph-node mapping and image-guided resection of swine tumors were performed using injection of ICG, of the NIR fluorophore HSA800 and of quantum dots. HSA800 was similarly considered herein for mapping all draining nodes, compared to larger-sized tracers that better outline one primary node.

Intraoperative imaging applications have thus largely demonstrated the feasibility and flexibility of fluorescence imaging use in the operating room. Conversely, nonspecific dyes,

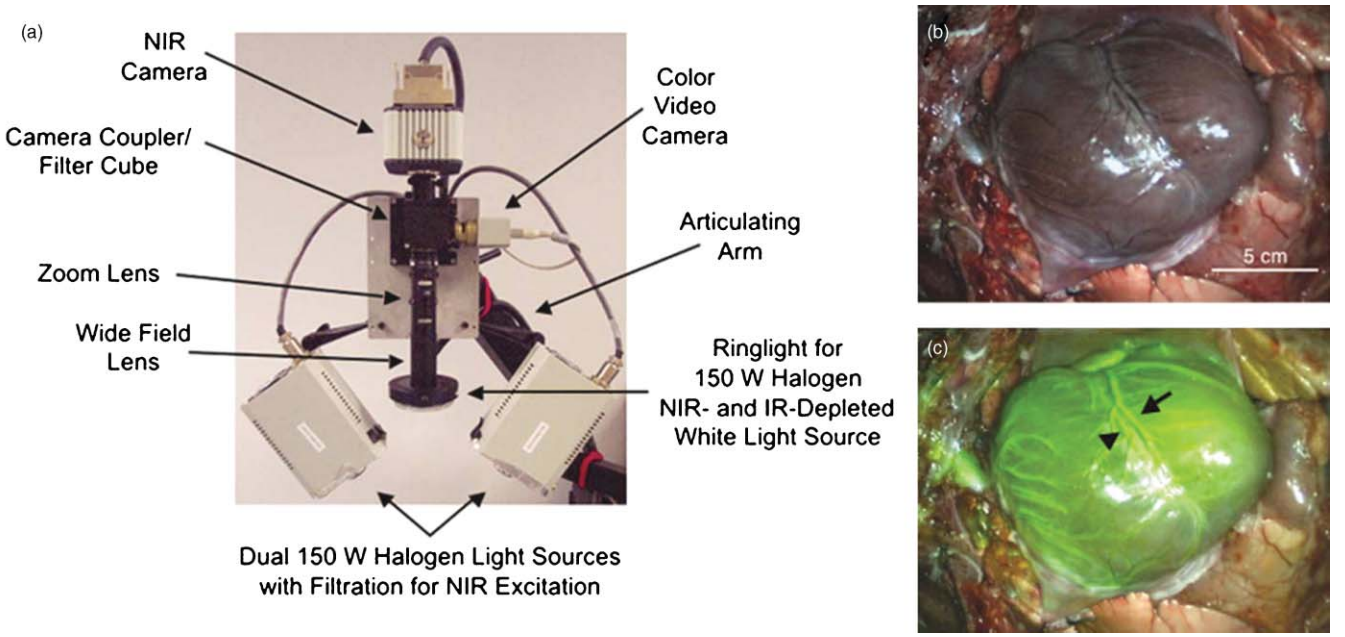

Fig. 3 Concurrent anatomy and NIR fluorescence imaging system for surgical guidance: (a) Architecture of imaging module. Fluorescence excitation light is provided using two halogen sources with appropriate filtration. NIR- and IR-depleted white light is supplied by ring light connected to a halogen source. (b) Color video image of surgeon's view. (c) Same color image with the pseudocolored overlay of the NIR fluorescence. The image shows intravascular mapping of the coronary circulation using ICG on a heart of a pig. The artery and vein are indicated by an arrow and arrowhead, respectively.

combined with the qualitative nature of photographic and video epi-illumination imaging systems have not yet allowed for high surgical impact, because these feasibility studies did not generally generate statistically important samples demonstrating improved surgical outcome or did not reach sufficient quantitative ability or image fidelity, although they may be particularly useful in interrogation of physiology. For this reason, a second generation of targeted contrast and advanced imaging systems was considered for improving the identification of disease, as described in the next section.

3 Imaging of Induced Porphyrins

Similarly to the Kuroiwa et al. study,[9] Stummer et al.[19] employed a modified surgical microscope (Zeiss OPMI CS-NC, Germany) to operate in fluorescence mode for fluorescence-guided tumor removal. The study imaged protoporphyrin IX (PpIX) induced endogenously at the site of malignant gliomas by administering 5-aminolevulinic acid (ALA) at a dose of 20 mg/kg at 3 h before induction of anesthesia. PpIX has characteristic red emission peaks at 635 and 704 nm under UV/blue-light excitation. A xenon light source coupled to the microscope, which can be switched from normal white light to violet-blue excitation light (375–440 nm), was employed in the study, whereas for optimum light delivery, a commercial liquid light guide was used to deliver ~ 40 mW/cm^2 irradiance at a distance of 5 cm from its tip. Transmission characteristics of excitation and fluorescence filters were chosen to transmit part of the remitted excitation light. Thereby, the observer retained an impression of tissue detail, next to tumor porphyrin fluorescence. Detection was achieved by an integrating three-chip CCD camera optimized for red-light detection. A series of studies[5,6,19] on >100 patients observed that removing "solidly fluorescing" tissue improved patient survival. It was further seen that residual tissue exhibiting "vague fluorescence" represented infiltrating tumor of intermediate or low cellular density. Overall, the potential of ALA-PpIX fluorescence-guided resection was demonstrated, but the overall impact of the methodology was limited by two facts, i.e., that only a single ALA dose and time interval was used and that the assessment of the tissue fluorescence was qualitative and subjective.

To further study the potential of induced porphyrin-assisted intraoperative imaging, Stummer et al.[20] launched a multicenter prospective-randomized clinical phase-III-trial in Germany, wherein 322 patients aged 23–73 years with suspected malignant glioma were randomly assigned to two groups (i.e., conventional brain surgery using white light or to fluorescence-guided surgery). The interim trial on 270 patients evaluated resections as defined by pre- and postoperative magnetic resonance imaging (MRI), and studied the impact of resection on progression-free survival, neurological morbidity, and overall survival. The study demonstrated almost a doubling of complete resections of glioma tumors in fluorescence-guided surgery, leading into longer progression-free patient survival compared to conventional microsurgery under white light. More recent studies confirm improved surgery outcome and patient survival (16.7 versus 11.8 months, $P < 0.0001$).[21,22]

4 Spectral Imaging

To improve on the detection accuracy of porphyrins, or other fluorochromes used in intraoperative application, spectral fluorescence imaging (SFI) was considered for glioma resection.[23,24] In this technique, imaging at five spectral bands (495, 543, 600,

640, and 720 nm; each band of 20 nm fullwidth at half maximum) was performed, utilizing a long working distance (~50 cm), 3-cm FoV, large depth of field (~2 cm), and high spatial resolution (~150 μm). Illumination was provided from a 50-W mercury lamp, which is filtered for 405 ± 15 nm excitation wavelength. Fluorescence signals were collected by the same lens used for illumination and were separated with a 50:50 beamsplitter to an imaging path and a fluorescence spectroscopy path that could obtain measurements from a point on the tissue surface. Images were detected using a CCD camera, and spectral separation was achieved using a filter wheel containing five different bandpass filters, which were rotated in front of the CCD camera. Tissue autofluorescence at 640 ± 20 nm was calculated by linearly interpolating the fluorescence spectra in the 600 ± 20 and 710 ± 20 nm bands and employed to improve the contrast of red Photofrin fluorescence centered at ~640 nm. However, the utilization of the complete spectral features of the system in the clinical studies, imaging patients administered with Photofrin and undergoing photodynamic therapy, was limited by slow acquisition times (tens of seconds). It was also found that blood vessels and hyperemic regions affected the imaging accuracy, because image artifacts were present due to variations in tissue optical properties not related to malignancy. Furthermore, the frequent switching between the SFI system and the surgical microscope complicated operations.

In general, spectral imaging has shown advantages in separating and better identifying target fluorochromes, and this technology has the potential to improve the performance of intraoperative imaging.[25] Recently, real-time multispectral systems (color and other spectral bands) have been reported for three-camera intraoperative imaging.[26,27] The system by Themelis et al.[27] attains the potential for real-time attenuation correction, based on spectral information, as described in the following. Therefore, besides the subtraction of autofluorescence, SFI can be employed in ways that correct also for optical property variations and improve the imaging accuracy.

5 Imaging Using Quantum Dots

Quantum dots have also been considered for intraoperative procedures. Frangioni and colleagues have investigated the use of quantum dots to assess lymphatic drainage from the site of the primary tumor.[17,18,28–30] The sentinel lymph-node concept states that if the first lymph node to receive lymphatic drainage from a tumor site (the sentinel node) does not contain tumor cells, it is unlikely that the tumor has metastasized to the lymphatic system. Several studies have indicated that, in several cancers (for example, breast cancer or melanoma), the sentinel lymph node accurately reflects the tumor status of regional nodes. Identification of the sentinel node is typically achieved by the use of radioactive tracers (Technetium 99 m) using a γ camera and the injection of a blue dye that can help in the visual identification of the node. To avoid the use of radioactivity and the inability of blue dyes to be detected when deep in tissue, Kim et al. demonstrated the utility of intraoperative epi-illumination fluorescence imaging to locate sentinel lymph nodes 1 cm deep in tissue,[28] in several locations, including the pleural space,[16,29] esophagus[17] or lung[30] of pigs[16,17,28,30] and rats.[16,29] The quantum dots employed for injection in these applications attained a hydrodynamic diameter of 15–20 nm, fluorescence emission at 840–860 nm, an aqueous quantum yield >13%, and a stable oligomeric phosphine coating for avoiding photobleaching. These quantum dots permitted imaging of sentinel lymph-node drainage in real time using excitation fluence rates of 5 mW/cm^2 and concentrations in the subnanomole range. Quantum dots remained localized to the subcapsular and intermediate sinuses of the sentinel lymph nodes. The particle size of the tracer used eventually determines the migration time in sentinel lymph-node mapping. Particles of <5 nm partition into blood, and those between 5 and 10 nm can migrate through nodal tissue often, resulting in false positives, whereas those >1000 nm largely remain at the injection site. The major limitation of the use of quantum dots concerns their potential toxicity because they contain heavy metals at their cores. The authors of these studies observed no evidence of acute toxicity.[17,18,28–30] Although most of the injected dose is removed by resecting nodal tissue, so toxicity may in fact be negligible, their use in humans may be problematic.

6 Imaging Viral Replication

An alternative to imaging extrinsically administered dyes and nanoparticles or induced fluorescence has recently emerged via the use of virally induced contrast. In particular, the use of a genetically modified oncolytic HSV (NV1066) carrying the transgene encoding for enhanced GFP was considered for accurate delineation of primary or metastatic cancer cells because the virus has shown selective infection of and replication in cancer cells. This approach results in highly cancer-specific expression of GFP that can identify even small foci of malignant tissue; however, clinical propagation requires careful consideration of biosafety issues.

Using a fluorescence laparoscopic and endoscopic system, Adusumilli et al. demonstrated that a single dose of NV1066, administered either locally (intratumoral or intracavity) or systemically, detected locoregional and distant disease throughout the body.[31] The imaging apparatus, co-developed with Olympus America, Inc. (Olympus America, Scientific Equipment Division, Melville, New York) imaged in both bright-field and fluorescent modes permitting the detection of GFP. Using this system, minimal residual disease following cytoreductive surgery and improvement of the completeness of cure-intended resection in mice was showcased.[31] Detection of breast cancer lymph-node metastases in mice[32,33] and detection of many kinds of tumors and metastases, such as peritoneal carcinomatosis, pancreatic cancer, colorectal cancer, gastric cancer, lung cancer, pleural disease, etc., in mice and hamsters, was also shown.[34] Figure 4 shows an example of expressed green fluorescence in lymphatic metastases by NV1066 injection. Possible contamination of GFP signals by tissue autofluorescence was avoided by appropriate filtering around the maximum of the GFP emission wavelengths.

7 Magneto-Fluorescent Nanoparticles

Multimodal nanoparticles or other dual-labeled contrast agents that attain contrast for both MRI and optical methods have been used to permit preoperative MR visualization and intraoperative fluorescence imaging. This strategy combines the superior whole-body imaging ability using MR with high-resolution

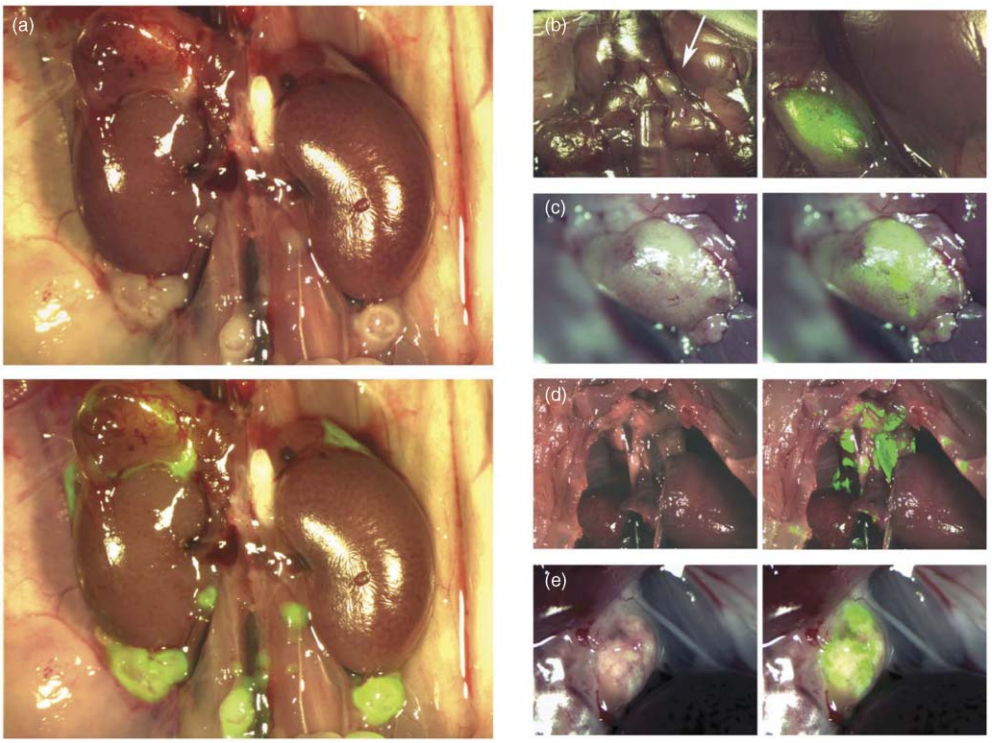

Fig. 4 Intraoperative imaging of enhanced GFP from lymphatic metastases of a mouse by infection with NV1066, an oncolytic herpes vector. Metastases in the paraaortic lymph nodes as well as adrenal metastases were revealed (a). Fluorescent endoscopic examination also revealed the location of metastases in (b) cervical, (c) axillary, (d) mediastinal, and (e) celiac lymph nodes from lung, breast, and gastric cancers, respectively.

fluorescence imaging in intraoperative environments. Magnetic nanoparticles (10–100 nm) have long blood half-lives because they are too large to undergo renal elimination and too small to be easily recognized by phagocytes. They are eventually internalized, predominantly by cells of the reticuloendothelial system, and their superparamagnetic iron is dissolved and joins normal iron pools. In response to these issues, long-circulating magnetic nanoparticles have been investigated as magnetic resonance contrast agents, with the hope of proving better delineation of brain tumors. It is also possible to conjugate the nanoparticles with other molecules to manufacture "targeted probes" (i.e., particles with specificity to specific cellular components) or for colabeling them to create dual-label contrast agents and probes, for example, using fluorescence labels matched to desired surgical applications.

Kircher et al.[35] explored a multimodal (NIR fluorescent and magnetic) nanoparticle based on a cross-linked iron oxide (CLIO) as a preoperative MRI contrast agent and intraoperative optical probe using a model of rat gliosarcoma with stably GFP-expressing 9L glioma cells. Noninvasive optical imaging was performed on rats implanted with 5 μL of the 9L-GFP-gliosarcoma cell suspension (10^6 cells in Hank's Buffered Salt Solution) in the striatum at a depth of 3 mm from the dural surface using a custom-built multispectral photographic imaging system (Siemens Medical Systems, Germany). They obtained images of a rat after craniotomy and exposition of the tumor, 24 h after i.v. injection of CLIO nanoparticles conjugated with the Cy5.5 fluorescent dye (GE Healthcare Life Sciences; former Amersham BioSciences). In addition to Cy5.5 images, white-light images were obtained for spatial colocalization of fluorescence images with anatomical features, whereas images acquired in the GFP channel served as the gold standard for delineation of true tumor extent. Figure 5 shows brain tumor margin delineation by Cy5.5-CLIO and congruent GFP signals. Using microscopy, they also found that Cy5.5-CLIO was strongly associated with CD11b-positive cells (microglia and macrophages) and less with GFP-positive cells (tumor cells). The approach further demonstrated the potential of linking preoperative MR findings with intraoperative procedures using the same contrast method.

Recently, Koyama et al.[36] synthesized and tested a single-polyamidoamine dendrimer-based hybrid probe, using gadolinium and the Cy5.5 fluorochrome for dual MR and nearinfrared imaging, respectively, also allowing pre- and intraoperative localization of the sentinel lymph node. They injected the agent into mammary glands of 10 normal mice to examine the lymphatic drainage from the breast. Immediately after the MRI scan, they performed an NIR optical imaging study with the commercial Maestro spectroscopic imaging unit (CRI, Waltham, Massachusetts) using an excitation 615–665 bandpass filter and an emission 700-nm long-pass filter. Because of interfering fluorescence from the injection site, the supraclavicular or lateral thoracic nodes close to the injection site could not be readily detected even though they were readily identified on the MRI. However, once the skin was removed, all sentinel lymph node were easily identified and resected under NIR image-guided surgery.

8 Fluorescence Imaging with Labeled Cells

Other targeted approaches with fluorescence-labeled carriers have also been considered for surgical applications. Flaumenhaft

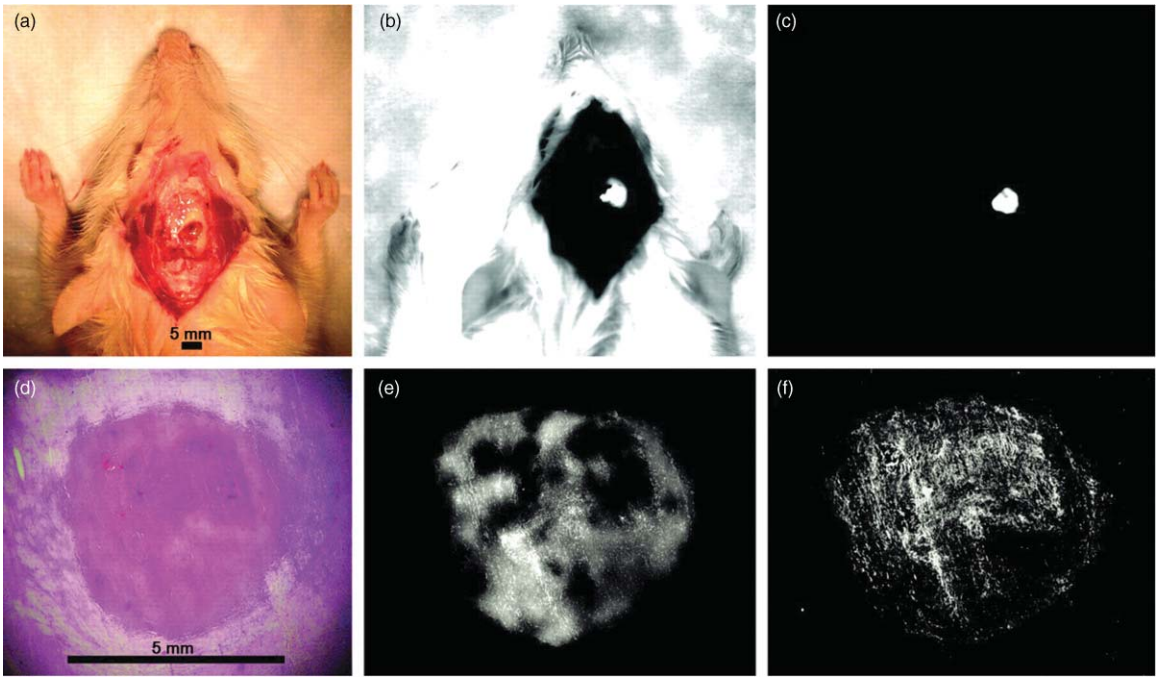

Fig. 5 Intraoperative brain tumor delineation with multimodal nanoparticle. After intravenous injection of Cy5.5-CLIO, i.e., fluorescent nanoparticle, a rat bearing GFP expressing 9L glioma tumor was imaged with (a) white light, (b) GFP channel, and (c) Cy5.5 channel, intraoperatively. After tumor resection, histological finding (D) and fluorescence microscopy at GFP (e) and Cy5.5 (f) channel on tumor tissue were performed. Cy5.5 fluorescence from nanoparticle clearly visualizes the tumor, as indicated by the correlation with the tumor extent as determined by GFP fluorescence.

et al.[37] imaged thrombus formation in the coronary, carotid, and femoral vessels of pigs in real time using IR-786-labeled platelets that fluoresced at 800 nm. The observations attained a signal-to-background ratio $\geq$2 maintained for at least 2 h. The imaging system utilized three CCD cameras and separated three spectral bands, using two dichroic mirrors, allowing color imaging (400–680 nm) and imaging of two distinct fluorochromes at 700–725 and >795-nm spectral bands.[37] The ability to image at two common spectral bands allows the use of popular fluorescent labels without the need to switch filters as would be the case if a single camera was utilized for fluorescence imaging. It was also possible therefore to assess blood flow by imaging methylene blue that fluoresced at 700 nm. The light source in this case consisted of 800 light-emitting diodes (LEDs) in a low-profile unit comprised of square modules. Each module was roughly 25 $\times$ 25 mm and housed 20 LEDs, driven by custom-designed, scalable electronics and utilizing a cooling system to dissipate heat generated by the LEDs. The source was contained in a sterile drape and generated fluence rates of 12.5–25 mW/cm^2 to excite the two fluorochromes and supply white-light illumination. With this approach, platelet-rich, actively growing clots were monitored and quantified with respect to size and kinetics after injury to vessels, cutaneous incisions, intravascular stent insertion, or introduction of embolic coils.

9 Fluorescence Imaging with Labeled Probes

Although significant volume of work has been performed with the use of intrinsic tissue contrast or with nonspecific fluorescent dyes or nanoparticles, there is high potential to employ new classes of dyes developed for targeted tumor imaging in order to improve intraoperative imaging. Antibody, antibody fragment, peptide, and minibody-based fluorescent probes can, for example, improve the detection ability of tumor borders (margins) or metastatic microfoci by attaching to upregulated cancer receptors[38–40] although such agents have not been explicitly considered only for surgical imaging applications, they can truly revolutionize the intraoperative and endoscopic imaging capacity by dramatically increasing the sensitivity and specificity of detection over human vision. Similarly, engineered probes can capitalize on tumor-specific physiological or molecular parameters, such as an active intracellular transport or enzymatic upregulation.[39–43] For example, activatable probes with sensitivity to tumoral proteases have been shown to accumulate at tumor margins where local inflammatory responses degrade the quenched dyes and activate fluorescence.[44]

The use of labeled molecules with tissue specificity is expected to become a crucial platform in the propagation of fluorescence surgical imaging into the clinic. Yet, regulatory procedures need to be followed before the clinical administration of these agents, which makes this process slow or even occasionally forbidding due to the associated cost and risk. However, there is potential to work closely with the administrative agencies and with labeled agents of known safe toxicity profiles to enable what could become a shift in the surgical paradigm.

10 Toward Accurate Fluorescence Imaging

Although photographic and video-imaging methods as described in the above appear attractive for surgical imaging the fluorescence imaging performance can be compromised by three major parameters, i.e., the depth of the fluorescence activity, the variation in tissue optical properties, and tissue

auto fluorescence. In the near-infrared, photon diffusion and fluorochrome depth complicate the imaging outcome by attenuating the fluorescence signal and by reducing the resolution. Tissue autofluorescence (i.e., fluorescence emerging from native tissue fluorochromes, such as collagen or NADH) may reduce the contrast available from a targeted fluorochrome. Systems that utilize imaging at multiple wavelengths have the potential to differentiate autofluorescence from a fluorochrome of interest, although the spectral response of a fluorochrome may be affected by depth, which can complicate the spectral unmixing process. In principle, dyes with different lifetime than that of tissue could be used for improving detection. However, this approach requires significantly more complex and expensive instrumentation. In addition, lifetime measurements, although insensitive to the optical attenuation they depend on the depth of the dye and its biochemical environment. Therefore, surgical imaging based on lifetime measurements may be practically challenging.

The spatial variation of tissue optical properties can also compromise the performance of photographic fluorescence imaging. For example, fluorescence activity in or under absorbing areas, such as a highly vascular tumor, is nonlinearly attenuated as a function of blood concentration and may show darker than in surrounding normal tissue, which may contain less fluorochrome but emit more light due to having overall less optical attenuation compared to the vascular tumor. Similarly, small fluorochrome amounts in a semitransparent or nonabsorbing lesion, for example, a cyst or a lymph node, may appear brighter on images compared to surrounding muscle containing similar amounts of fluorochrome. These effects are typically corrected in tomographic systems[45] but have not been thoroughly addressed in systems developed for surgical imaging applications.

These limitations of photographic imaging have been noted[27,46,47] and are exemplified in Fig. 6. An approach to improve on imaging performance in this case is the utilization of measurements at multiple wavelengths. It has, for example, been shown possible to collect data at three channels[27] [Fig. 6(a)], i.e., a fluorescence channel, a light absorption channel, and a color channel, and to implement image-correction algorithms for the variation of optical absorption by tissue in real time, yielding more accurate images of a surgical field in the presence of hypo-/hyperemic or hypoxic areas as appropriate for intraoperative surgical imaging. The principle of operation is based on independently measuring background attenuation images/video that can normalize the fluorescence images/video captured in a separate channel. Bogaards et al.[47] have also proposed different ratio implementations for intraoperative fluorescence imaging that offer a combination of fluorescence measurements, or fluorescence and intrinsic measurements, and have demonstrated improvements over conventional epi-illumination imaging. Overall, methods that improve on the limitations of conventional photographic fluorescence imaging or video will become important as the clinical translation of such approaches is considered.

11 Imaging of Intrinsic Signals

In addition to imaging-induced or extrinsically administered agents, intrinsic tissue contrast (i.e., native light-tissue interactions) is also considered for intraoperative procedures. For example, optical imaging of neuronal activity has been considered for evaluating damage during neurosurgical resection, as an alternative or surrogate method to functional MRI and electrocortical stimulation mapping.[48] Changes of neuronal activity can be detected as absorption changes due to corresponding variation in blood volume and oxygenation during functional activity, as well as scattering changes due to ion fluxes between neurons and glia, resulting in cell volume changes. This contrast has been used for studying functional organization in the cat or monkey visual cortex,[49] the rodent somatosensory cortex,[50] or the human cortex in cognitively evoked functional activity[51] and functional brain mapping studies in humans.[52–54]

Another approach utilizes optical coherence tomography (OCT), a technique that can offer high resolution images (1–10 μ) of tissue structure at depths up to 1–2 mm. The primary OCT contrast generation mechanism is backscattered light from tissue structures, attributed to tissue scattering. Concurrent improvement of laser sources, beam-delivery instruments, detection schemes, and research techniques has brought significant technological advance of OCT. As a result, OCT has been clinically demonstrated in a diverse set of medical specialties, including ophthalmology, oncology, or cardiology[55] and its application for intraoperative imaging has also been gaining attention.[56–59] In ophthalmology, OCT was initially demonstrated for cross-sectional retinal imaging in 1991.[60] Since then, it has become a key diagnostic tool in the ophthalmology community. Several trials for surgical guide and intraoperative management with OCT have been also evaluated. Azzolini et al. showed the usefulness of OCT to identify macular membrane in idiopathic epiretinal macular membrane surgery.[61] To improve the precision of refractive surgery, Bagayev et al. showed that the use of OCT with a specially developed algorithm of signal processing for determination of the removed corneal thickness profile *in situ* with laser ablation is more promising compared to the use of the reflected component.[58] Intraoperative OCT may also allow the identification of tissue borders and the identification of submucosal tumor growth. OCT may be especially effective in detecting human breast lesions due to significant structural differences between the fibro-fatty tissue comprising most of the breast and the densely scattering tumor tissue that comes of from the functional epithelial network of ducts and lobules. Boppart et al. demonstrated this potential in rat mammary tumor models[62] and also studied the detection of human breast cancer *ex vivo* with portable real-time OCT.[63]

Brown et al. imaged the radial arteries and saphenous veins of 35 patients scheduled for coronary artery bypass grafting using catheter-based OCT *in situ* prior to harvesting vessels and *ex vivo* after vessel excision.[64] OCT reliably demonstrated luminal abnormalities within bypass conduits resulted from atherosclerosis, trauma, or retention of thrombi. They showed the feasibility of OCT in cardiac surgery as a selection tool of conduit vessels in spite of limited tissue penetration depth and blood-induced signal attenuation. Li et al. also demonstrated OCT of normal and osteoarthritic cartilage during open knee surgery,[65] in real time, achieving 11-μm resolution at 4 fps. The study was performed on six patients and showed detection of structural changes including cartilage thinning and fibrillations.

Other optical sensing approaches included spectroscopic identification of cancerous signatures with point-to-point single-fiber detection; however, this technique has not yet been shown

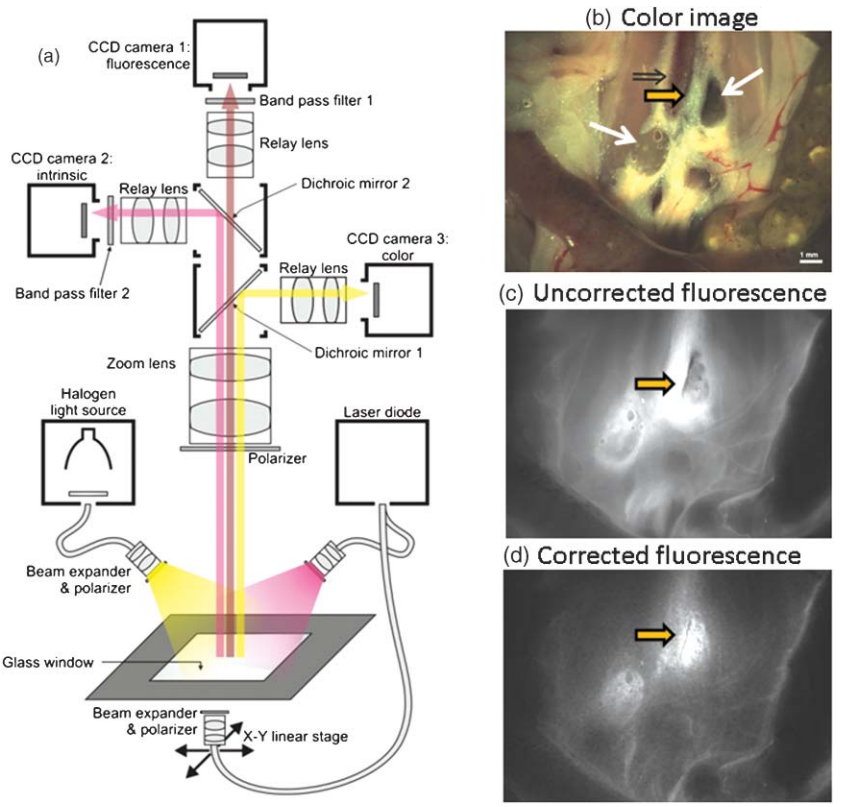

Fig. 6 (a) Schematic of the imaging system developed to operate in real-time (video) mode and implementing concurrent fluorescence, attenuation (intrinsic), and color measurements. All optical path lengths from the lens to the cameras are equal (not plotted in scale on the drawing). A transillumination branch is also implemented in the system for volumetric imaging. (b) Postmortem color image of a surgically exposed mouse abdominal area in epi-illumination mode. The two white arrows show the lumbar lymph nodes injected with a mixture of Cy5.5 fluorescence dye and India Ink, around the inferior *vena cava* (double-line arrow). The orange arrow indicates an area of adipose tissue. (c) Raw fluorescence image showing low signal intensity from the lymph nodes compared to bright background signals due to internal light attenuation due to the India ink but increased fluorescence intensity from the adipose tissue, due to scattering of fluorescent light escaping laterally from the nodes. (d) Normalized image showing markedly improved fluorescence quantification, correctly resolving the underlying fluorescence activity in the nodes. Reproduced from Ref. 27.

to be practical for high-throughput intraoperative application, although it demonstrates the possibility of translation from probe-based spectroscopy to macroscopic spectral imaging.[66–69]

Finally, a surgical approach that has benefited from conventional optical imaging and has been met with strong interest is the use of optically guided robotic-assisted surgery,[70] the most popular technology being the Da Vinci system (Intuitive Surgical Inc., Sunnyvale, California).[71–73] The Da Vinci system combines a stereo endoscope with highly articulated robotic arms that can translate surgical procedures into minimally invasive environments. In this case, the surgeon operates the robotic arms on a console, while viewing high-resolution images of the surgical site on a monitor. In this manner, the Da Vinci system can offer improved laparoscopy procedures and has found use in pelvic surgery, including prostate, rectal, uterine, and cervix operations[71] or cardiac and gynecologic surgical procedures.[72,73]

12 Optoacoustic Imaging and Surgery

The recent emergence of various optoacoustic imaging approaches open further possibilities in photonic imaging, including surgical optical imaging. Visualization of blood vessels has been demonstrated[74] and can be of importance in vascular surgery and in identifying vital functional structures during tumor removal. Multispectral optoacoustic tomography (MSOT), a method developed to spectrally identify photoabsorbing agents, such as fluorochromes or nanoparticles[75,76] is another optoacoustic method that can bring benefits to surgical imaging. The ability to detect molecular probes based on their spectral signature is of particular importance when using targeted or activatable probes because typically, such agents need to be allowed to distribute for several minutes to hours in order to preferentially target cancer and activate or clear from the circulation. Therefore, it would be impractical to monitor such agents as absorption changes; instead, real-time MSOT would be required for practical detection.[77] Optoacoustic imaging has also been considered in detecting lymph nodes[78,79] in small animals, and depending on the light penetration conditions, such application could also find clinical applications for superficial nodes.

From a practical standpoint, the application of optoacoustics to cancer delineation may require contact with tissue, which could limit the application and FoV that can be surveyed. Conversely, optoacoustics can yield high-resolution imaging within several millimeters to centimeters of depths in tissues and can

become a very useful add-on to survey capable systems, such as epi-illumination fluorescence imaging.

13 Summary and Outlook

Despite the highly invasive nature of many tumors, surgery remains a common therapeutic approach in oncology. Mounting literature reports however confirm the inaccuracy of oncological surgery procedures.[80–82] Improvements in the resection technique are therefore highly sought to improve survival, decrease functional loss, and increase the quality of life of the cancer patient.[83] Over the years, a variety of dyes and systems have been employed to improve margin resection. Since the original use of fluorescein in the 1940s and 1950s[1,2] several fluorochromes or fluorescent photosensitizers have been investigated for their ability to enhance margin delineation, including porphyrins,[5,6] ICG,[3] and fluorescein-albumin.[4] Investigations using fluorescein also continued.[7] Importantly, tumor-targeting approaches[39–41] can significantly enhance the specificity of detection and improve the surgical outcome. Yet, new probes with the potential to improve cancer imaging need to be evaluated as to their toxicity and biodistribution, which presents a significant challenge as to their clinical translation.

Despite promising results, it has been noted that conventional fluorescence detection based on photographic imaging lacks the ability to accurately characterize fluorescence in tissues as it offers crude observations[6,24] because it does not account for variations in the detected fluorescence intensity as a function of tissue optical property variations or the fluorochrome depth. Therefore, the ability to offer accurate, artifact-free imaging, in real-time mode, has been identified as an important improvement for fluorescence-guided tumor surgery and accurate margin identification.[24,27,46,47] In response, different approaches are emerging for improving imaging performance in fluorescence surgical imaging. Focus is given to imaging in the NIR to avoid interference with standard color imaging, reduce tissue autofluorescence, and enable sensitivity at greater depths. In addition, quantification is improved by using spectral schemes that can decompose true fluorescence signals from other tissue contributions. Small FoV, high-resolution approaches, such as OCT or confocal and two-photon microscopy can also bring benefits to surgical imaging; however, large FoV methods, such fluorescence imaging, may be, regardless, required to guide higher-resolution methods. Point-detection spectroscopic approaches have also been considered for surgical cancer identification[66–68] but they cannot assess the extent of tumor infiltration; in this case, hyperspectral imaging approaches appear more appropriate for accurate tumor margin resection and overall intraoperative operation.

Surgical optical imaging ties well with the surgeon's perception of the disease and attains several attractive features, including a practical integration in the operating room due to the small form factor, low cost, and high-detection sensitivity and resolution for surface and subsurface detection. Compared therefore to other imaging modalities, it attains high dissemination potential and can find widespread clinical propagation in many surgical oncology fields and beyond, including head and neck cancer, otolaryngology, neurooncology, gynaecologic oncology, urology, and thoracic surgery. It is also possible to combine optical imaging approaches and other imaging methods, in multimodal approaches, for example, using nuclear medicine methods, ultrasound imaging, or navigation methods based on whole-body radiological images, to overall improve the procedures and surgical ability. Furthermore, optical imaging techniques are expected to be useful not only for real-time intraoperative procedures but also for postoperative inspection of excised tissues, resulting in more efficient and less time-consuming examinations compared to histopathological analyses.

Evolving fluorescence enhanced surgical vision has the potential to shape the future of surgical procedures by improving the sensitivity and accuracy of tumor delineation (circumferential resection margin), locoregional involvement, and lymph-node interrogation. It is therefore anticipated that the technology of dedicated intraoperative optical instrumentation and the employment of targeted agents will significantly grow in the future to allow for improved surgical outcome using optical imaging, i.e., a method with highly attractive characteristics to allow for high dissemination and wide acceptance into the operating room.

References

1. G. E. Moore, W. T. Peyton, S. W. Hunter, and L. French, "Sodium fluorescein and radioactive diiodofluorescein in the localization of tumors of the central nervous system," *Abstracts World Surg., Obstet., Gynaecol.* **5**, 351–352 (1940).
2. G. E. Moore, C. M. Caudill, J. F. Marvin, J. B. Aust, S. N. Chou, and G. A. Smith, "Clinical and experimental studies of intracranial tumors with fluorescein dyes with an additional note concerning the possible use of K42 and iodine 131 tagged human albumin," *Am. J. Roentgenol. Radium. Ther. Nucl. Med.* **66**, 1–8 (July 1951).
3. M. M. Haglund, M. S. Berger, and D. W. Hochman, "Enhanced optical imaging of human gliomas and tumor margins," *Neurosurgery* **38**, 308–317 (February 1996).
4. P. Kremer, A. Wunder, H. Sinn, T. Haase, M. Rheinwald, U. Zillmann, F. K. Albert, and S. Kunze, "Laser-induced fluorescence detection of malignant gliomas using fluorescein-labeled serum albumin: experimental and preliminary clinical results," *Neurol. Res.* **22**, 481–489 (July 2000).
5. W. Stummer, S. Stocker, S. Wagner, H. Stepp, C. Fritsch, C. Goetz, A. E. Goetz, R. Kiefmann, and H. J. Reulen, "Intraoperative detection of malignant gliomas by 5-aminolevulinic acid-induced porphyrin fluorescence," *Neurosurgery* **42**, 518–525; discussion 525–526 (March 1998).
6. W. Stummer, A. Novotny, H. Stepp, C. Goetz, K. Bise, and H. J. Reulen, "Fluorescence-guided resection of glioblastoma multiforme by using 5-aminolevulinic acid-induced porphyrins: a prospective study in 52 consecutive patients," *J. Neurosurg.* **93**, 1003–1013 (December 2000).
7. M. Kabuto, T. Kubota, H. Kobayashi, T. Nakagawa, H. Ishii, H. Takeuchi, R. Kitai, and T. Kodera, "Experimental and clinical study of detection of glioma at surgery using fluorescent imaging by a surgical microscope after fluorescein administration," *Neurol. Res.* **19**, 9–16 (February 1997).
8. T. Desmettre, J. Devoisselle, and S. Mordon, "Fluorescence properties and metabolic features of indocyanine green (ICG) as related to angiography," *Surv. Ophthalmol.* **45**, 15–27 (2000).
9. T. Kuroiwa, Y. Kajimoto, and T. Ohta, "Development of a fluorescein operative microscope for use during malignant glioma surgery: a technical note and preliminary report," *Surg. Neurol.* **50**, 41–48; discussion 48–49 (July 1998).
10. M. M. Haglund, D. W. Hochman, A. M. Spence, and M. S. Berger, "Enhanced optical imaging of rat gliomas and tumor margins," *Neurosurgery* **35**, 930–940; discussion 940–941 (November 1994).
11. C. Holm, M. Mayr, E. Hofter, A. Becker, U. J. Pfeiffer, and W. Muhlbauer, "Intraoperative evaluation of skin-flap viability using laser-induced fluorescence of indocyanine green," *Br. J. Plast. Surg.* **55**, 635–644 (December 2002).

12. K. Kubota, J. Kita, M. Shimoda, K. Rokkaku, M. Kato, Y. Iso, and T. Sawada, "Intraoperative assessment of reconstructed vessels in living-donor liver transplantation, using a novel fluorescence imaging technique," *J. Hepatobiliary Pancreat. Surg.* **13**, 100–104 (2006).
13. M. Takahashi, T. Ishikawa, K. Higashidani, and H. Katoh, "SPY: an innovative intra-operative imaging system to evaluate graft patency during off-pump coronary artery bypass grafting," *Interact. Cardiovasc. Thorac. Surg.* **3**, 479–483 (September 2004).
14. A. Nakayama, F. del Monte, R. J. Hajjar, and J. V. Frangioni, "Functional near-infrared fluorescence imaging for cardiac surgery and targeted gene therapy," *Mol. Imaging* **1**, 365–377 (October 2002).
15. A. M. De Grand and J. V. Frangioni, "An operational near-infrared fluorescence imaging system prototype for large animal surgery," *Technol. Cancer Res.Treat*. **2**, 553–562 (December 2003).
16. C. P. Parungo, S. Ohnishi, A. M. De Grand, R. G. Laurence, E. G. Soltesz, Y. L. Colson, P. M. Kang, T. Mihaljevic, L. H. Cohn, and J. V. Frangioni, "*In vivo* optical imaging of pleural space drainage to lymph nodes of prognostic significance," *Ann. Surg. Oncol.* **11**, 1085–1092 (December 2004).
17. C. P. Parungo, S. Ohnishi, S. W. Kim, S. Kim, R. G. Laurence, E. G. Soltesz, F. Y. Chen, Y. L. Colson, L. H. Cohn, M. G. Bawendi, and J. V. Frangioni, "Intraoperative identification of esophageal sentinel lymph nodes with near-infrared fluorescence imaging," *J. Thorac. Cardiovasc. Surg.* **129**, 844–850 (April 2005).
18. E. Tanaka, H. S. Choi, H. Fujii, M. G. Bawendi, and J. V. Frangioni, "Image-guided oncologic surgery using invisible light: completed preclinical development for sentinel lymph node mapping," *Ann. Surg. Oncol.* **13**, 1671–1681 (December 2006).
19. W. Stummer, H. Stepp, G. Moller, A. Ehrhardt, M. Leonhard, and H. J. Reulen, "Technical principles for protoporphyrin-IX-fluorescence guided microsurgical resection of malignant glioma tissue," *Acta Neurochir. (Wien)* **140**, 995–1000 (1998).
20. W. Stummer, U. Pichlmeier, T. Meinel, O. D. Wiestler, F. Zanella, and H. J. Reulen, "Fluorescence-guided surgery with 5-aminolevulinic acid for resection of malignant glioma: a randomised controlled multicentre phase III trial," *Lancet Oncol.* **7**, 392–401 (May 2006).
21. W. Stummer, H. Reulen, T. Meinel, U. Pichlmeier, W. Schumacher, J. Tonn, V. Rohde, F. Oppel, B. Turowski, C. Woiciechowsky, K. Franz, and T. Pietsch, "Extent of resection and survival in glioblastoma multiforme: identification of and adjustment for bias," *Neurosurgery* **62**, 564–576 (2008).
22. W. Stummer, J. Tonn, H. Mehdorn, U. Nestler, K. Franz, C. Goetz, A. Bink, and U. Pichlmeier, "Counterbalancing risks and gains from extended resections in malignant glioma surgery: a supplemental analysis from the randomized 5-aminolevulinic acid glioma resection study," *J. Neurosurg.* (April 14, 2010, Epub ahead of print).
23. V. X. Yang, P. J. Muller, P. Herman, and B. C. Wilson, "A multispectral fluorescence imaging system: design and initial clinical tests in intra-operative Photofrin-photodynamic therapy of brain tumors," *Lasers Surg. Med.* **32**, 224–232 (2003).
24. A. Bogaards, A. Varma, S. P. Collens, A. Lin, A. Giles, V. X. Yang, J. M. Bilbao, L. D. Lilge, P. J. Muller, and B. C. Wilson, "Increased brain tumor resection using fluorescence image guidance in a preclinical model," *Lasers Surg. Med.* **35**, 181–190 (2004).
25. R. M. Levenson and J. R. Mansfield, "Multispectral imaging in biology and medicine: slices of life," *Cytometry A* **69**, 748–758 (August 1, 2006).
26. S. Troyan, V. Kianzad, S. Gibbs-Strauss, S. Gioux, A. Matsui, R. Oketokoun, L. Ngo, A. Khamene, F. Azar, and J. Frangioni, "The FLARE intraoperative near-infrared fluorescence imaging system: a first-in-human clinical trial in breast cancer sentinel lymph node mapping," *Ann. Surg. Oncol.* **16**(10), 2943–2952 (2009).
27. G. Themelis, J. Yoo, K. Soh, R. Schulz, and V. Ntziachristos, "Real-time intraoperative fluorescence imaging system using light-absorption correction," *J. Biomed. Opt.* **14**, 064012 (2009).
28. S. Kim, Y. T. Lim, E. G. Soltesz, A. M. De Grand, J. Lee, A. Nakayama, J. A. Parker, T. Mihaljevic, R. G. Laurence, D. M. Dor, L. H. Cohn, M. G. Bawendi, and J. V. Frangioni, "Near-infrared fluorescent type II quantum dots for sentinel lymph node mapping," *Nat. Biotechnol.* **22**, 93–97 (January 2004).
29. C. P. Parungo, Y. L. Colson, S. W. Kim, S. Kim, L. H. Cohn, M. G. Bawendi, and J. V. Frangioni, "Sentinel lymph node mapping of the pleural space," *Chest* **127**, 1799–1804 (May 2005).
30. E. G. Soltesz, S. Kim, R. G. Laurence, A. M. DeGrand, C. P. Parungo, D. M. Dor, L. H. Cohn, M. G. Bawendi, J. V. Frangioni, and T. Mihaljevic, "Intraoperative sentinel lymph node mapping of the lung using near-infrared fluorescent quantum dots," *Ann. Thorac. Surg.* **79**, 269–277; discussion 269-277 (January 2005).
31. P. S. Adusumilli, D. P. Eisenberg, Y. S. Chun, K. W. Ryu, L. Ben-Porat, K. J. Hendershott, M. K. Chan, R. Huq, C. C. Riedl, and Y. Fong, "Virally directed fluorescent imaging improves diagnostic sensitivity in the detection of minimal residual disease after potentially curative cytoreductive surgery," *J Gastrointest. Surg.* **9**, 1138–1146; discussion 1146–1147 (November 2005).
32. D. P. Eisenberg, P. S. Adusumilli, K. J. Hendershott, S. Chung, Z. Yu, M. K. Chan, M. Hezel, R. J. Wong, and Y. Fong, "Real-time intraoperative detection of breast cancer axillary lymph node metastases using a green fluorescent protein-expressing herpes virus," *Ann. Surg.* **243**, 824–830; discussion 830–832 (June 2006).
33. P. S. Adusumilli, D. P. Eisenberg, B. M. Stiles, S. Chung, M. K. Chan, V. W. Rusch, and Y. Fong, "Intraoperative localization of lymph node metastases with a replication-competent herpes simplex virus," *J. Thorac. Cardiovasc. Surg.* **132**, 1179–1188 (November 2006).
34. P. S. Adusumilli, B. M. Stiles, M. K. Chan, D. P. Eisenberg, Z. Yu, S. F. Stanziale, R. Huq, R. J. Wong, V. W. Rusch, and Y. Fong, "Real-time diagnostic imaging of tumors and metastases by use of a replication-competent herpes vector to facilitate minimally invasive oncological surgery," *FASEB J.* **20**, 726–728 (April 2006).
35. M. F. Kircher, U. Mahmood, R. S. King, R. Weissleder, and L. Josephson, "A multimodal nanoparticle for preoperative magnetic resonance imaging and intraoperative optical brain tumor delineation," *Cancer Res.* **63**, 8122–8125 (December 1, 2003).
36. Y. Koyama, V. S. Talanov, M. Bernardo, Y. Hama, C. A. Regino, M. W. Brechbiel, P. L. Choyke, and H. Kobayashi, "A dendrimer-based nanosized contrast agent dual-labeled for magnetic resonance and optical fluorescence imaging to localize the sentinel lymph node in mice," *J. Magn. Reson. Imaging* **25**, 866–871 (April 2007).
37. R. Flaumenhaft, E. Tanaka, G. J. Graham, A. M. De Grand, R. G. Laurence, K. Hoshino, R. J. Hajjar, and J. V. Frangioni, "Localization and quantification of platelet-rich thrombi in large blood vessels with near-infrared fluorescence imaging," *Circulation* **115**, 84–93 (January 2, 2007).
38. A. M. Wu and T. Olafsen, "Antibodies for molecular imaging of cancer," *Cancer J.* **14**, 191–197 (2008).
39. R. Weissleder and M. Pittet, "Imaging in the era of molecular oncology," *Nature* **452**, 580–589 (2008).
40. R. Tsien, "Building and breeding molecules to spy on cells and tumors," *FEBS Lett.* **579**, 927–932 (February 7, 2005).
41. S. Achilefu, "Lighting up tumors with receptor-specific optical molecular probes," *Technol. Cancer Res. Treat* **3**, 393–409 (2004).
42. P. Zou, S. Xu, S. Povoski, A. Wang, M. Johnson, E. Martin Jr., V. Subramaniam, R. Xu, and D. Sun, "Near-infrared fluorescence labeled anti-tag-72 monoclonal antibodies for tumor imaging in colorectal cancer xenograft mice," *Mol. Pharm.* **6**, 428–440 (2009).
43. R. Xu, J. Huang, J. Xu, D. Sun, G. Hinkle, E. Martin, and S. Povoski, "Fabrication of indocyanine green encapsulated biodegradable microbubbles for structural and functional imaging of cancer," *J. Biomed. Opt.* **14**, 034020 (2009).
44. A. A. Bogdanov, Jr., C. P. Lin, M. Simonova, L. Matuszewski, and R. Weissleder, "Cellular activation of the self-quenched fluorescent reporter probe in tumor microenvironment," *Neoplasia* **4**, 228–236 (May-June 2002).
45. R. Weissleder and V. Ntziachristos, "Shedding light onto live molecular targets," *Nat. Med.* **9**, 123–128 (January 2003).
46. V. Ntziachristos, G. Turner, J. Dunham, S. Windsor, A. Soubret, J. Ripoll, and H. Shih, "Planar fluorescence imaging using normalized data," *J. Biomed. Opt.* **10**, 064007 (2005).
47. A. Bogaards, H. J. Sterenborg, J. Trachtenberg, B. C. Wilson, and L. Lilge, "*In vivo* quantification of fluorescent molecular markers in real-time by ratio imaging for diagnostic screening and image-guided surgery," *Lasers Surg. Med.* **39**, 605–613 (August 2007).
48. N. Pouratian, A. F. Cannestra, N. A. Martin, and A. W. Toga, "Intraoperative optical intrinsic signal imaging: a clinical tool for functional brain mapping," *Neurosurg. Focus* **13**, e1 (October 15, 2002).

49. A. Shmuel and A. Grinvald, "Functional organization for direction of motion and its relationship to orientation maps in cat area 18," *J. Neurosci.* **16**, 6945–6964 (November 1, 1996).
50. I. Yazawa, S. Sasaki, H. Mochida, K. Kamino, Y. Momose-Sato, and K. Sato, "Developmental changes in trial-to-trial variations in whisker barrel responses studied using intrinsic optical imaging: comparison between normal and de-whiskered rats," *J. Neurophysiol.* **86**, 392–401 (July 2001).
51. M. M. Haglund, G. A. Ojemann, and D. W. Hochman, "Optical imaging of epileptiform and functional activity in human cerebral cortex," *Nature* **358**, 668–671 (August 20, 1992).
52. K. Sato, T. Nariai, S. Sasaki, I. Yazawa, H. Mochida, N. Miyakawa, Y. Momose-Sato, K. Kamino, Y. Ohta, K. Hirakawa, and K. Ohno, "Intraoperative intrinsic optical imaging of neuronal activity from subdivisions of the human primary somatosensory cortex," *Cereb. Cortex* **12**, 269–280 (March 2002).
53. T. H. Schwartz, L. M. Chen, R. M. Friedman, D. D. Spencer, and A. W. Roe, "Intraoperative optical imaging of human face cortical topography: a case study," *Neuroreport* **15**, 1527–1531 (June 28, 2004).
54. M. M. Haglund and D. W. Hochman, "Imaging of intrinsic optical signals in primate cortex during epileptiform activity," *Epilepsia* **48** (Suppl 4), 65–74 (2007).
55. A. M. Zysk, F. T. Nguyen, A. L. Oldenburg, D. L. Marks, and S. A. Boppart, "Optical coherence tomography: a review of clinical development from bench to bedside," *J. Biomed. Opt.* **12**, 051403 (September-October 2007).
56. S. A. Boppart, M. E. Brezinski, C. Pitris, and J. G. Fujimoto, "Optical coherence tomography for neurosurgical imaging of human intracortical melanoma," *Neurosurgery* **43**, 834–841 (October 1998).
57. A. V. Shakhov, A. B. Terentjeva, V. A. Kamensky, L. B. Snopova, V. M. Gelikonov, F. I. Feldchtein, and A. M. Sergeev, "Optical coherence tomography monitoring for laser surgery of laryngeal carcinoma," *J. Surg. Oncol*. **77**, 253–258 (August 2001).
58. S. N. Bagayev, V. M. Gelikonov, G. V. Gelikonov, E. S. Kargapoltsev, R. V. Kuranov, A. M. Razhev, I. V. Turchin, and A. A. Zhupikov, "Optical coherence tomography for in situ monitoring of laser corneal ablation," *J. Biomed. Opt.* **7**, 633–642 (October 2002).
59. S. Rais-Bahrami, A. W. Levinson, N. M. Fried, G. A. Lagoda, A. Hristov, Y. Chuang, A. L. Burnett, and L. M. Su, "Optical coherence tomography of cavernous nerves: a step toward real-time intraoperative imaging during nerve-sparing radical prostatectomy," *Urology* **72**, 198–204 (February 15, 2008).
60. D. Huang, E. A. Swanson, C. P. Lin, J. S. Schuman, W. G. Stinson, W. Chang, M. R. Hee, T. Flotte, K. Gregory, C. A. Puliafito, and J. G. Fujimoto, "Optical coherence tomography," *Science* **254**, 1178–1181 (November 22, 1991).
61. C. Azzolini, F. Patelli, M. Codenotti, L. Pierro, and R. Brancato, "Optical coherence tomography in idiopathic epiretinal macular membrane surgery," *Eur. J. Ophthalmol.* **9**, 206–211 (July-September 1999).
62. S. A. Boppart, W. Luo, D. L. Marks, and K. W. Singletary, "Optical coherence tomography: feasibility for basic research and image-guided surgery of breast cancer," *Breast Cancer Res. Treat*. **84**, 85–97 (March 2004).
63. F. T. Nguyen, A. M. Zysk, J. G. Kotynek, F. J. Bellafiore, K. M. Rowland, P. A. Johnson, J. E. Chaney, and S. A. Boppart, "Portable real-time optical coherence tomography system for intraoperative imaging and staging of breast cancer," *Proc. SPIE* **6430**, 64300H (2007).
64. E. N. Brown, N. S. Burris, J. Gu, Z. N. Kon, P. Laird, S. Kallam, C. M. Tang, J. M. Schmitt, and R. S. Poston, "Thinking inside the graft: applications of optical coherence tomography in coronary artery bypass grafting," *J. Biomed. Opt.* **12**, 051704, (September-October 2007).
65. X. Li, S. Martin, C. Pitris, R. Ghanta, D. L. Stamper, M. Harman, J. G. Fujimoto, and M. E. Brezinski, "High-resolution optical coherence tomographic imaging of osteoarthritic cartilage during open knee surgery," *Arthritis Res. Ther.* **7**, R318–323 (2005).
66. G. Bottiroli, A. C. Croce, D. Locatelli, R. Nano, E. Giombelli, A. Messina, and E. Benericetti, "Brain tissue autofluorescence: an aid for intraoperative delineation of tumor resection margins," *Cancer Detect. Prev.* **22**, 330–339 (1998).
67. W. C. Lin, S. A. Toms, M. Johnson, E. D. Jansen, and A. Mahadevan-Jansen, "*In vivo* brain tumor demarcation using optical spectroscopy," *Photochem. Photobiol.* **73**, 396–402 (April 2001).
68. S. A. Toms, W. C. Lin, R. J. Weil, M. D. Johnson, E. D. Jansen, and A. Mahadevan-Jansen, "Intraoperative optical spectroscopy identifies infiltrating glioma margins with high sensitivity," *Neurosurgery* **57**, 382–391; discussion 382–391 (October 2005).
69. S. C. Gebhart, R. C. Thompson, and A. Mahadevan-Jansen, "Liquid-crystal tunable filter spectral imaging for brain tumor demarcation," *Appl. Opt.* **46**, 1896–1910 (April 1, 2007).
70. H. Kim and P. Schulam, "The PAKY, HERMES, AESOP, ZEUS, and da Vinci robotic systems," *Urol. Clin. North. Am.* **31**, 659–669 (2004).
71. S. Wexner, R. Brgamaschi, A. Lacy, J. Udo, H. Brölmann, R. Kennedy, and H. John, "The current status of robotic pelvic surgery: results of a multinational interdisciplinary consensus conference," *Surg. Endosc.* **23**, 438–443 (2009).
72. P. Modi, E. Rodriguez, and W. J. Chitwood, "Robot-assisted cardiac surgery," *Interact Cardiovasc. Thorac. Surg.* **9**, 500–505 (2009).
73. L. Mettler, T. Schollmeyer, J. Boggess, J. Magrina, and A. Oleszczuk, "Robotic assistance in gynecological oncology," *Curr. Opin. Oncol.* **20**, 581–589 (2008).
74. X. Wang, Y. Pang, G. Ku, X. Xie, G. Stoica, and L. V. Wang, "Noninvasive laser-induced photoacoustic tomography for structural and functional *in vivo* imaging of the brain," *Nat. Biotechnol.* **21**, 803–806 (July 2003).
75. D. Razansky, M. Distel, C. Vinegoni, R. Ma, N. Perrimon, R. Koester, and V. Ntziachristos, "Imaging of Mesoscopic Targets using Selective-Plane Optoacoustic Tomography," *Nat. Photon.* **3**, 412–417 (2009).
76. V. Ntziachristos and D. Razansky, "Molecular imaging by means of multi-spectral opto-acoustic tomography (MSOT)," *ACR Chem. Rev.* **110**, 2783–2794 (2010).
77. V. Ntziachristos, "Going deeper than microscopy: the optical imaging frontier in biology," *Nat. Methods* **7**, 603–614 (2010).
78. C. Kim, K. Song, F. Gao, and L. Wang, "Sentinel lymph nodes and lymphatic vessels: noninvasive dual-modality *in vivo* mapping by using indocyanine green in rats—volumetric spectroscopic photoacoustic imaging and planar fluorescence imaging," *Radiology* **255**, 442–450 (2010).
79. T. Erpelding, C. Kim, M. Pramanik, L. Jankovic, K. Maslov, Z. Guo, J. Margenthaler, M. Pashley, and L. Wang, "Sentinel lymph nodes in the rat: noninvasive photoacoustic and US imaging with a clinical US system," *Radiol.* **256**, 102–110 (2010).
80. R. Bergamaschi, P. Pessaux, P. Burtin, and J. Arnaud, "Abdominoperineal resection for locally recurrent rectal cancer," *Tech. Coloproctol* **5**, 97–102 (2001).
81. L. Gilbeau, G. Kantor, E. Stoeckle, P. Lagarde, L. Thomas, M. Kind, P. Richaud, J. M. Coindre, F. Bonichon, and B. N. Bui, "Surgical resection and radiotherapy for primary retroperitoneal soft tissue sarcoma," *Radiother. Oncol.* **65**, 137–143 (2002).
82. C. Verbeke, D. Leitch, K. V. Menon, M. J. McMahon, P. J. Guillou, and A. Anthoney "Redefining the R1 resection in pancreatic cancer," *Br. J. Surg.* **93**, 1232–1237 (2006).
83. M. K. Bucci, A. Maity, A. J. Janss, J. B. Belasco, M. J. Fisher, Z. A. Tochner, L. Rorke, L. N. Sutton, P. C. Phillips, and H. K. Shu, "Near complete surgical resection predicts a favorable outcome in pediatric patients with nonbrainstem, malignant gliomas: results from a single center in the magnetic resonance imaging era," *Cancer* **101**, 817–824 (August 15, 2004).